Sol−Gel Syntheses and Spectroscopic Characterization of Chromium-Doped Silicates and Germanates

P. Sujatha Devi,[†,‡] H. D. Gafney,*[,‡] V. Petricevic,[§] R. R. Alfano,[§] D. He,[||] and K. E. Miyano[||]

Sol-Gel Division, Central Glass and Ceramic Research Institute, Calcutta 700 032, India; Departments of Chemistry and Biochemistry, Queens College, The City University of New York, 65-30 Kissena Boulevard, Flushing, New York 11367; Department of Physics, The City College and Graduate School of the City University of New York, 138th Street at Convent Avenue, New York, New York 10031; and Department of Physics, Brooklyn College, The City University of New York, 2900 Bedford Avenue, Brooklyn, New York 11210

Received November 12, 1999. Revised Manuscript Received March 6, 2000

To avoid the technical difficulties encountered with high-temperature processing techniques, low-temperature sol−gel processes have been examined as routes to the Cr-doped olivine, Mg_2SiO_4, and the structural analogues Ca_2SiO_4 and Ca_2GeO_4. Gelation yields transparent, lightly colored gels that are converted to microcrystalline ceramic powders on heating to 850 °C. Initially doped with $CrCl_3 \cdot 6H_2O$ (0.01−1%), conversion to the ceramic is accompanied by changes in the coordination and oxidation state of the chromium. Consistent with size considerations, EPR, EXAFS, and XANES data indicate chromium exists principally as tetrahedrally coordinated Cr^{4+} in Ca_2SiO_4 and Ca_2GeO_4, and as a mixture of octahedrally coordinated Cr^{3+} and tetrahedrally coordinated Cr^{4+} in Cr-Mg_2SiO_4. Visible and near-IR electronic absorption and emission spectra reflect the composition of the material, and a comparison of the absorption of randomly oriented microcrystalline ceramics shows a surprising similarity in both band position and shape to polarized absorptions of forsterite single crystals.

1. Introduction

The need to minimize material dispersion in optical communications has focused attention on solid-state materials that exhibit tunable laser emissions in the near-IR region. Cr(IV), in particular, has been incorporated in several crystalline hosts and examined for laser action.[1−6] Current data indicate that those Cr(IV) systems that luminesce in the near-IR, such as the olivine-based forsterite, contain Cr(IV) in a distorted tetrahedral site.[7−13] This site provides a low-symmetry field thought to be necessary for near-IR emission and laser action.[9−13]

Forsterite and other olivine systems have been prepared by high-temperature processing techniques,[11−15] coprecipitation,[16] and different sol−gel routes.[17−21] Systems that are isostructural with forsterite, Mg_2SiO_4, also exhibit near-IR emissions.[9,10,14] Forsterite, Mg_2SiO_4 has an orthorhombic structure with the space group *Pbnm* and contains four formula units per unit cell. In the unit cell, Mg^{2+} ions occupy two distinct octahedral coordination sites, M_1 with inversion symmetry (C_i) and M_2 with

* To whom correspondence should be addressed. E-mail: hgafney@qc1.qc.edu.
† Currently on leave of absence from CG&CRI, Calcutta, India, to Queens College, The City University of New York.
‡ Queens College.
§ City College.
|| Brooklyn College.

(1) Petricevic, V.; Gayen, S. K.; Alfano, R. R. *Appl. Phys. Lett.* **1988**, *53*, 2590.
(2) Petricevic, V.; Gayen, S. K.; Alfano, R. R.; Yamagishi, K.; Anzai, H.; Yamaguchi, Y. *Appl. Phys. Lett.* **1988**, *52*, 1040.
(3) Verdun, H. R.; Thomas, L. M.; Andrauskas, D. M.; McCollum, T.; Pinto, A. *Appl. Phys. Lett.* **1988**, *53*, 2593.
(4) Eiless, H.; Dennis, W. M.; Yen, W. M.; Kuck, S.; Petermann, K.; Huber, G.; Jiu, W. *IEEE J. Quantum Electron.* **1993**, *29*, 2508.
(5) Deka, C.; Chai, B. H. T.; Shimony, Y.; Chany, X. X.; Munin, E.; Bass, M. *Appl. Phys. Lett.* **1992**, *61*, 2141.
(6) Kuck, S.; Petermann, K.; Pohlmann, U.; Schonhoff, U.; Huber, G. *Appl. Phys. B* **1994**, *58*, 153.
(7) Pollock, C. R.; Barber, D. B.; Mass, J. L.; Markgraf, S. *IEEE J. Quantum Electron.* **1995**, *1*, 62.
(8) Carrig, T. J.; Pollock, C. R. *J. Quantum Electron.* **1993**, *29*, 2835.
(9) Yang, L.; Petricevic, V.; Alfano, R. R. *Novel Laser Sources and Applications*; Becker, J. F., Tam, A. C., Gruber, J. B. Lam, L., Eds.; SPIE Proceedings Nov 12−13, 1993, San Jose, CA; p 103.
(10) Petricevic, V.; Seas, A.; Alfano, R. R.; Kokta, M. R.; Randles, M. H.; Paper A.T.E1-1 presented at the Advanced Solid-state Lasers Conference, New Orleans, LA, Feb 2−4, 1993.
(11) Petricevic, V.; Gayen, S. K.; Alfano, R. R. *OSA Proceeding on Tunable Solid State Lasers*; Shand, M. L. Jenssen, H. P., Eds.; Optical Society of America: Woodbury, NY, 1989; Vol. 5, p 77.
(12) Eiless, H.; Hommerich, U. S.; Jacobsen, M.; Yen, W. M. *Chem. Phys. Lett.* **1993**, *212*, 109.
(13) Reinen, D.; Kesper, U.; Atanasov, M.; Roos, J. *Inorg. Chem.* **1995**, *34*, 184.
(14) Hazenkamp, M. F.; Oetliker, U.; Gudel, H. U.; Kesper, U.; Reinen, D. *Chem. Phys. Lett.* **1995**, *233*, 466.
(15) Swamson, H. E.; Tarye, E. *Natl. Bur. Stand. (U. S.)* **1953**, *Circulation 539*, 83.
(16) Yamaguchi, O.; Nakayima, Y.; Shimira, K. *Chem. Lett.* **1976**, 401.
(17) Kazakos, A.; Komarneni, S.; Roy, R. *Mater. Lett.* **1990**, *9*, 405.
(18) Burlitch, J. M.; Beeman, M. L.; Riley, B.; Kohlstedt, D. L. *Chem. Mater.* **1991**, *3*, 692.
(19) Park, D. G.; Duchamp, J. C.; Duncan, T. M.; Burlitch, J. M. *Chem. Mater.* **1994**, *6*, 1990.
(20) Park, D. G.; Burlitch, J. M.; Geray, R. F.; Dieckmann, R.; Barber, D. B.; Pollock, C. R. *Chem. Mater.* **1993**, *5*, 518.
(21) Sujatha Devi, P.; Gafney, H. D.; Petricevi, V.; Alfano, R. R. *J. Non-Cryst. Solids.* **1996**, *203*, 78.

10.1021/cm990730+ CCC: $19.00
Published on Web 04/14/2000

mirror symmetry (C_s), while Si^{4+} occupies a tetrahedral coordination site.[22] Forsterite doped with Cr, Cr-Mg_2SiO_4, prepared by the sol−gel technique yields a mixture of Cr(III) and Cr(IV) with Cr(III) being the dominant oxidation state.[18−20] In Mg_2SiO_4, Cr is thought to occupy a Mg^{2+} site as octahederally coordinated Cr^{3+}, and a Si^{4+} site as tetrahedrally coordinated Cr^{4+}. Ca_2SiO_4 and Ca_2GeO_4, although not naturally occurring olivines, possess the olivine structure similar to forsterite, and hence for convenience, are referred to as olivines here. The similarity of the radii of Cr^{4+}, 0.41 Å, and the tetrahedrally coordinated Ge^{4+}, 0.39 Å, led to the selection of Ca_2GeO_4 as a possible matrix for Cr^{4+} stabilization since the size similarity might favor displacement of the Ge^{4+} and formation of tetrahedrally coordinated Cr^{4+}. Similarly, the larger difference between the ionic radius of Ca^{2+}, 1.00 Å, and Cr^{3+}, 0.62 Å, in Ca_2SiO_4 might inhibit the Cr^{3+} substitution of a Ca^{2+} site and promote Cr^{4+} occupation of a tetrahedral Si^{4+} site. To examine the possible implications of these size considerations, Cr-doped Ca_2GeO_4 and Ca_2SiO_4 have been prepared, and the spectroscopic properties of the gels and the resulting powders obtained on heating these gels are compared to those of Cr-doped Mg_2SiO_4. Technical difficulties encountered with high-temperature processing, specifically the preferential evaporation of the component oxides such as GeO_2 and the existence of polymorphic modifications, however, led to an examination of low-temperature sol−gel techniques to synthesize these olivine structured materials. X-ray absorption near-edge structure (XANES) studies confirm that changes in chromium oxidation state and coordination, consistent with the size expectations, occur on converting the gels to the corresponding microcrystalline ceramic. The visible and near-IR absorption spectra of the ceramic powders show a surprising similarity in both band energy and shape to the single-crystal, polarized absorption spectra of chromium-doped forsterite.

2. Experimental Section

Materials. Tetramethylorthosilane, $Si(OCH_3)_4$, (Aldrich, 99%), tetramethoxy germanium, $Ge(OCH_3)_4$ (Aldrich, 99%), magnesium methoxide, $Mg(OCH_3)_2$ (Aldrich, 10% by weight in methanol), calcium acetate monohydrate, $Ca(OOCCH_3)_2H_2O$ (Aldrich 99.9%), and $CrCl_3{\cdot}6H_2O$ (Fisher Scientific, 99.99%) were used as received.

Syntheses. *i.* Chromium-doped magnesium silicate, designated Cr-MS, was prepared by acid hydrolysis of a 2:1 mixture of $Mg(OCH_3)_2$ and $Si(OCH_3)_4$. A 107.6 mL aliquot of a methanol solution containing 10 wt % magnesium methoxide (0.128 mol) was added slowly to a mixture of 10 mL of TMOS (9.775 g, 0.064 mol) in 10 mL of methanol with stirring. The resulting mixture was stirred for 30 min to ensure homogeneity and then $CrCl_3{\cdot}6H_2O$ in 5 mL of methanol was added dropwise with stirring. Gelation of the resulting greenish-yellow solution was accomplished by the slow addition of 9.2 mL of distilled water and 1 mL of 1 M HCl. The ratio of water to alkoxide was maintained at 2.6:1 in all samples, whereas the Cr/Si ratio was varied from 0.01 to 1% by increasing the amount of $CrCl_3{\cdot}6H_2O$ added. All reaction mixtures were stirred in an ice bath for 2−3 h and then transferred to Teflon or glass containers, covered, and maintained at 30 ± 1 °C. Within 24 h, transparent, greenish-yellow gels formed.

ii. Chromium-doped calcium silicates, designated Cr-CS, were prepared by room-temperature acid hydrolysis of a 2:1 mixture of $Ca(OOCCH_3)_2$ and $Si(OCH_3)_4$. Ten milliliters of TMOS (9.775 g, 0.064 mol) in 10 mL of methanol was added slowly with stirring to 10 mL of a 2:1 H_2O:CH_3OH solution containing 22.552 gm of calcium acetate (0.128 mol). The solution was stirred for 30 min to ensure homogeneity and then a weight of $CrCl_3{\cdot}6H_2O$ corresponding to a Cr/Si mol ratio ranging from 0.01 to 0.1, was dissolved in 5 mL of methanol and added dropwise. Gelation of the greenish-yellow solution was catalyzed by the slow, dropwise addition of 1 mL of 1 M HCl. The solution was stirred in an ice bath for 30 min and then transferred to Teflon or glass containers, covered, and allowed to gel at 30 ± 1 °C. Transparent greenish-yellow gels were formed within 24 h.

iii. Chromium-doped calcium germanate gels, designated Cr-CG, were prepared in a similar manner. Ten milliliters of $Ge(OCH_3)_4$ (0.038 mol) in 5 mL of methanol was mixed with 10 mL of a 2:1 mixture of water and methanol containing 13.390 gm of calcium acetate. The mixture was stirred for 30 min in an ice bath and 5 mL of methanol containing a weight of $CrCl_3{\cdot}6H_2O$ corresponding to Cr/Ge ratio ranging from 0.01 to 1 was added followed by 0.5 mL of 1 M HCl. The resulting green solution was stirred for 2.5 h in an ice bath and then transferred to Teflon or glass containers, covered, and allowed to gel at room temperature, 22 ± 1 °C. Transparent, greenish gels formed within 24 h.

After drying and aging for 2 weeks at room temperature, all xerogels were further dried by CO_2 supercritical extraction (Tousimis Samdri PVT-3B). The dried, extracted gels, which were highly transparent, but quite brittle, were calcined for 6 h at different temperatures up to1000 °C. All samples were heated at a rate of 1 °C/min in a Thermolyne model 46100 programmable oven.

Instrumentation. Thermogravimetric analysis (TGA) and differential thermal analyses (DTA) were performed on a Perkin-Elmer 7 Series system using Al_2O_3 as a reference material. All samples were heated in Pt crucibles at a rate of 10 °C/min. X-ray diffraction was performed on a Philips PW 1710 diffractometer using Cu Kα radiation at a scan rate of 2°/min. UV−visible−near-IR absorption spectra of the doped gels and ceramic powders were recorded on an Aviv model 14 spectrometer at a spectral resolution of ±0.25 nm. Electronic spectra of the gels were recorded in the transmission mode, while those of the doped ceramic powders were recorded with a diffuse reflectance accessory. All spectra were recorded relative to the undoped gel or its corresponding ceramic powder. Emission spectra were obtained by exciting solid samples with either 670 or 800 nm light from a chopped diode laser or at 1064 nm with a Nd:YAG laser. The near-IR emission was monitored through a 0.25 m monochromator with an uncooled Hamamatsu P394A PbS detector and SR530 lock-in amplifier. The monochromator is equipped with a grating blazed at 1000 nm. X-band electron paramagnetic resonance (EPR) spectra were recorded on a Bruker spectrometer at room temperature using MnO as an internal standard. "g" values were calculated as $g = h\gamma/\beta H$, where h is Planck's constant, γ is the spectrometer frequency, 9.76 GHz, β is the Bohr magneton, and H is the magnetic field in Gauss. Extended X-ray absorption fine structure (EXAFS) and XANES spectra of the Cr edge were recorded on the ×23A2 beamline at the National Synchroton Light Source at Brookhaven National Laboratory. Transmission and fluorescent yield spectra were acquired using a Si (311) double-crystal monochromator, ion chambers, and a Lytle fluorescence detector equipped with a vanadium filter.

3. Results

Heating Cr-doped MS, CS, and CG gels to 700 °C leads to weight losses of 33, 36, and 40%, respectively, with the majority of the weight loss, ∼20−25%, occurring below 200 °C. Each sample exhibits broad endothermic processes at ∼150 °C, suggesting that the dominant weight loss in this temperature range is the

(22) Rager, H.; Weiser, G. *Bull. Mineral.* **1981**, *104*, 603.

Table 1. Comparison of Lattice Parameters and Site Occupancies of the Studied Silicates and Germanates

	lattice parameters (Å)				site occupancies			
compound	*a*	*b*	*c*	crystal type	M_1	M_2	T_d	ref(s)
Mg_2SiO_4	4.758	10.205	5.960	orthorhombic	Mg^{2+}	Mg^{2+}	Si^{4+}	9
γ-Ca_2SiO_4	5.078	11.225	6.760	orthorhombic	Ca^{2+}	Ca^{2+}	Si^{4+}	9, 25
γ-Ca_2GeO_4	5.240	11.400	6.790	orthorhombic	Ca^{2+}	Ca^{2+}	Si^{4+}	14, 25

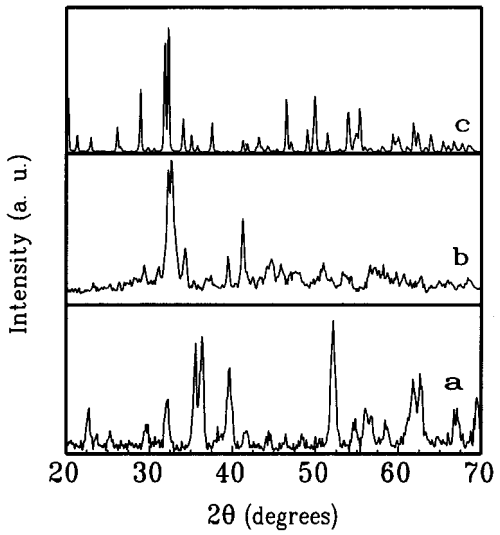

Figure 1. X-ray diffraction from the microcrystalline powders calcined at 850 °C: (a) Cr-Mg_2SiO_4 (Cr-MS), (b) Cr-Ca_2SiO_4 (Cr-CS), and (c) Cr-Ca_2GeO_4 (Cr-CG).

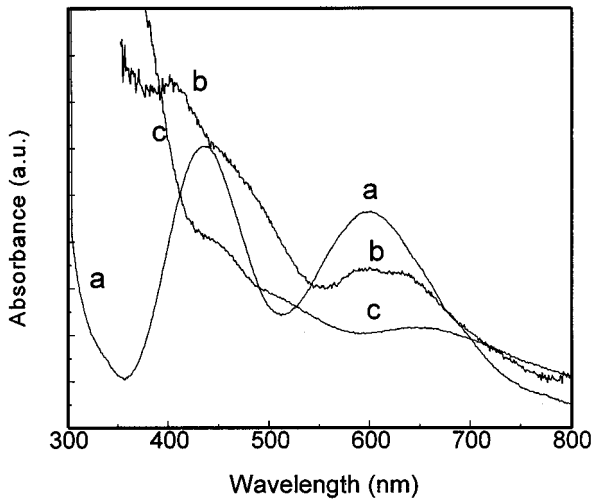

Figure 2. Absorption spectra of Cr-doped olivine gels: (a) Mg_2SiO_4, (b) Ca_2SiO_4, and (c) Ca_2GeO_4. All spectra are referred against undoped gels, and recorded at a bandwidth of 2 nm. Samples thickness is 2.0 mm.

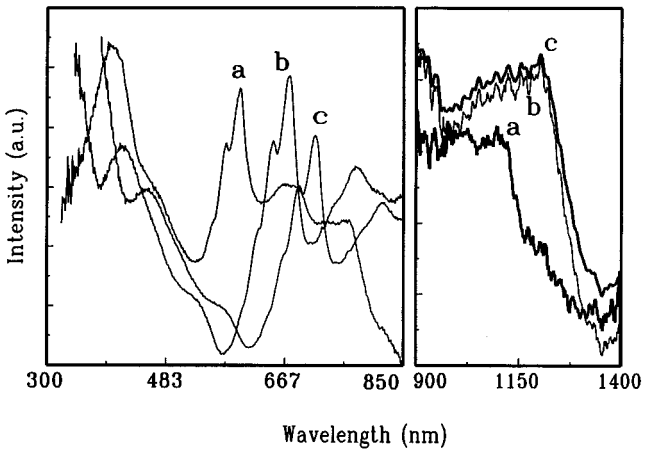

Figure 3. Reflectance spectra of Cr-doped olivine powders: (a) Mg_2SiO_4, (b) Ca_2SiO_4, and (c) Ca_2GeO_4.

removal of water and methanol from the gel net work.[18,20,21] Weak, broad exotherms occurring in the 350 °C region in each olivine gel are attributed to the combustion of organic groups that failed to hydrolyze during gelation, while weak exotherms at 720, 790, and 830 °C for Cr-MS, Cr-CS, and Cr-CG are attributed to transition from a transparent, amorphous glass to an opaque ceramic. A simultaneous change in color indicates an accompanying chemical change of the Cr(III) dopant. A 6-h calcination at 850 °C in air, for example, converts the transparent, light-green Cr-MS gel to a light-purple ceramic powder, while the Cr-CS and Cr-CG convert to light-green or bright bluish-green ceramics, respectively. Although calcination yields powder-like materials, each exhibits sharp X-ray reflections (Figure 1), confirming conversion to microcrystalline materials. The lattice parameters and site occupancies of the three compounds are given in Table 1.

Consistent with Cr(III) doping, absorption spectra of an aliquot of each of the doped sol were essentially identical to the spectra of the Cr(III) precursor solution with strong absorbances around 425 and 590 nm. The Cr-doped gels (Figure 2) also exhibit similar bands at 430 and 600 nm.

Heating to 850 °C converts each gel to a ceramic and replaces the broad, structureless bands of Cr^{3+} by more intense, well-resolved, sharp bands in the visible and weaker, broader bands in the near-IR (Figure 3). Other than differences in relative intensity, the near-IR absorptions are independent of the specific olivine host, whereas the visible transitions depend on the specific olivine. The latter bands appear in the 398−460 nm region with the maxima shifting from 398 nm in Cr-MS to 415 nm in Cr-CS and 456 nm in Cr-CG. A series of sharp bands with distinct higher energy shoulders appear at 604, 579, and 555 nm in Cr-MS; 677, 652, and 627 nm in Cr-CS; and 718, 694, and 663 nm in Cr-CG. Following these transitions are a series of broader absorptions with maxima at 754, 784, and 825 nm for Cr-MS, Cr-CS, and Cr-CG, and absorptions in the near-IR. Cr-CS and Cr-CG exhibit identical near-IR absorptions with maxima at 1207 nm, while Cr-MS exhibits a lower intensity band at 1092 nm (Figure 3).

Room-temperature samples of the Cr-doped gels fail to exhibit an emission in the visible or near-IR when excited with either 670- or 800-nm light whereas the corresponding ceramic powders, obtained by calcining at 850 °C in air are emissive (Figure 4a). Cr-doped Mg_2SiO_4 exhibits a lower intensity, broad band with a maximum at 950 nm, and a higher intensity, broad band with a maximum at 1158 nm (Figure 4a). Spectra of the Cr-doped Ca_2SiO_4 and Ca_2GeO_4, on the other hand, exhibit only lower energy transitions with maxima at 1275 and 1285 nm, (Figure 4b and c), respectively. At

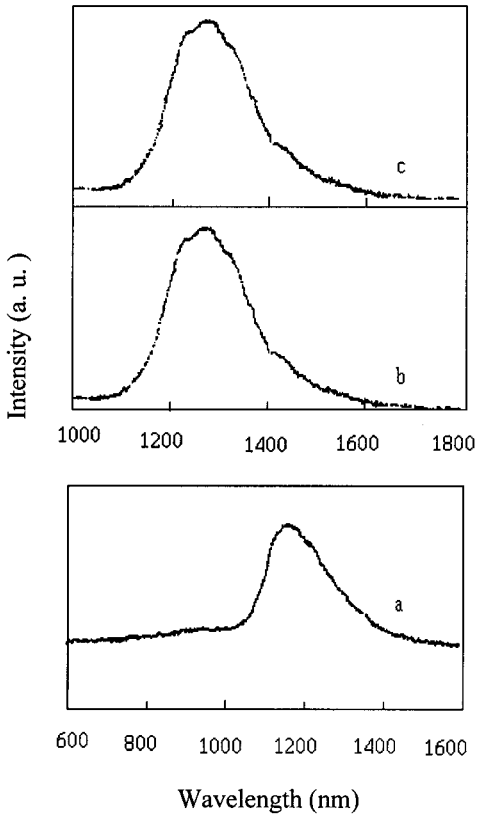

Figure 4. Room-temperature emission spectra of Cr-doped microcrystalline powders calcined at 850 °C: (a) Cr-Mg_2SiO_4, (b) Cr-Ca_2SiO_4, and (c) Cr-Ca_2GeO_4. All samples were excited with 670 nm light.

the same loading, i.e., Cr/Si or Cr/Ge of 0.01%, the 1275 and 1285 nm bands of Cr-Ca_2SiO_4 and Cr-Ca_2GeO_4 are significantly more intense than the 1158 nm emission from Cr-Mg_2SiO_4. The emission band maxima and bandwidth are independent of excitation with 670, 800, or 1064 nm light and hence the spectra recorded at 670 nm only is shown in Figure 4.

EPR spectra of Cr-MS at room temperature exhibit two prominent resonances, whereas Cr-CS and Cr-CG exhibit a single prominent resonance under the same conditions. Each sample exhibits a resonance with $g = 2.05 \pm 0.02$ and half width $\sim 200 \pm 10$ G (Figure 5). Weak shoulders in the low- and high-field regions are also evident in these spectra, but the intensity of the shoulder, relative to that of the prominent resonance, shows no correlation with the preparative conditions examined in these experiments. In addition to the $g = 2.05 \pm 0.02$ resonance, Cr-MS samples exhibit an additional low field resonance with $g \approx 5$.

To further probe the oxidation state and coordination of Cr in these olivine powders, two doped hosts, Cr-MS and Cr-CG, were examined by EXAFS and XANES. XANES data were recorded for the above samples at the Cr K-edge (Figures 6 and 7) and compared to that collected from the following standards: Cr metal, $CrCl_2$, Cr_2O_3, CrO_2, and CrO_3 (Figure 8). The latter were used as standards for the 0, 2+, 3+, 4+, and 6+ oxidation states of chromium, respectively, and their respective energy positions are listed in Table 2. We will use the term preedge to refer to the strong peak that occurs prior to the main absorption onset. The 4+ and 6+ standards exhibit a preedge peak around 5991 ± 3 and

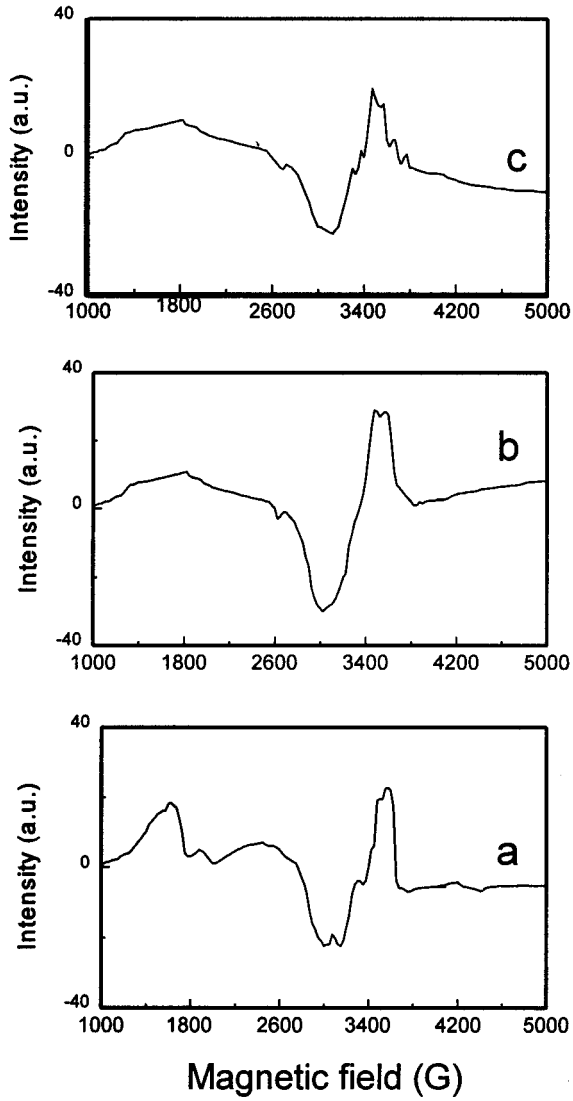

Figure 5. Room-temperature X-band EPR spectra of Cr-doped olivine powders: (a) Mg_2SiO_4, (b) Ca_2SiO_4, and (c) Ca_2GeO_4.

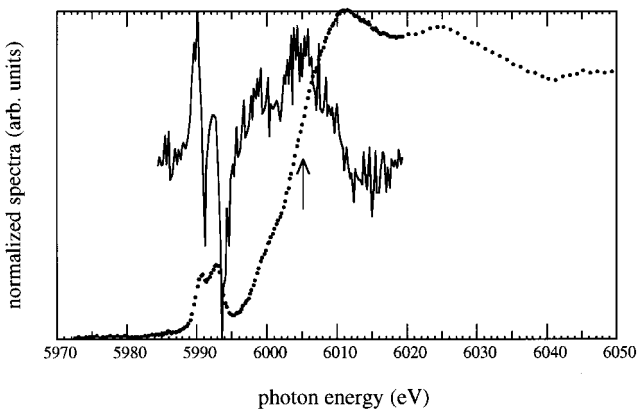

Figure 6. XANES at the Cr K-edge of Cr-doped Mg_2SiO_4. The arrow designates the edge position as determined from the first derivative.

5994 ± 3 eV, respectively. Cr-CG exhibits a narrow, but split preedge absorption at 5990 ± 3 eV, while Cr-MS shows a slightly broader split preedge feature at 5990 ± 4 eV. The preedge peak is followed by the main absorption edge, which appears in the first derivative spectrum and is shown by an arrow in the respective

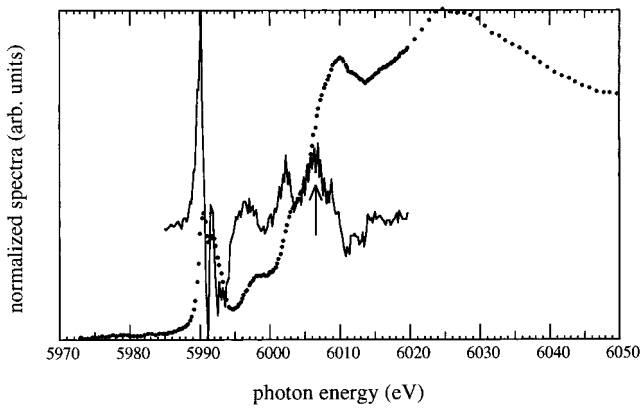

Figure 7. XANES at the Cr K-edge of Cr-doped Ca_2GeO_4. The arrow designates the edge position as determined from the first derivative.

Table 2. Edge Position versus the Oxidation States of Different Chromium Compounds

compound	oxidation state	main edge (eV)
Cr metal	0	5999.24
$CrCl_2$	+2	6004.13
Cr_2O_3	+3	6005.58
CrO_2	+4	6006.40
CrO_3	+6	6008.05
Mg_2SiO_4	+3, +4	6004.20, 6006.00
Ca_2GeO_4	+4	6006.50

spectrum (Figures 6 and 7). The main absorption edge is broad and lies at 6004 and 6006 eV for Cr-Mg_2SiO_4 (Figure 6) and 6006.5 eV for Cr-Ca_2GeO_4 (Figure 7).

4. Discussion

Consistent with an initial doping with $CrCl_3 \cdot 6H_2O$, each sol and dried gel exhibits bands at 430 and 600 nm (Figure 2), indicating the $^4A_2 \rightarrow {}^4T_1$ and $^4A_2 \rightarrow {}^4T_2$ transitions of octahedrally coordinated Cr^{3+}, respectively (Figure 9).[22−24] There is little change in band position or shape on going from the sol to the gel in a specific sample, but considerable variation from sample to sample. In different samples of Cr-MS sols and gels, for example, the band half-widths are larger than those found in aqueous solution, and the maximum of the $^4A_2 \rightarrow {}^4T_2$ transition ranges from 580 to 640 nm. Spectra of Cr-CS and Cr-CG gels exhibit similar band maxima, but the bands are noticeably broader and less resolved than those of Cr-MS, and the spectrum extends further into the near-IR. Since Ca^{2+} is larger than Mg^{2+}, the broadness of the transitions may reflect a wider variation in field strengths than that found in aqueous solution, but this fails to account for the absorption extending into the near-IR. It is possible that some of the chromium in the Ca_2SiO_4 and Ca_2GeO_4 gels is, at this point, present as tetrahedrally coordinated Cr(IV). However, the absence of conformation from the other experimental probes suggests that the amount present must be small.

Heating in air to 850 °C converts each gel to an opaque, ceramic powder. However, each powder exhibits sharp X-ray reflections (Figure 1), indicating their microcrystalline nature. Furthermore, there are no reflections indicative of SiO_2, MgO, CaO, GeO_2, or other olivine phases, indicating these ceramic powders are composed of single phases. Comparing the calculated *d*

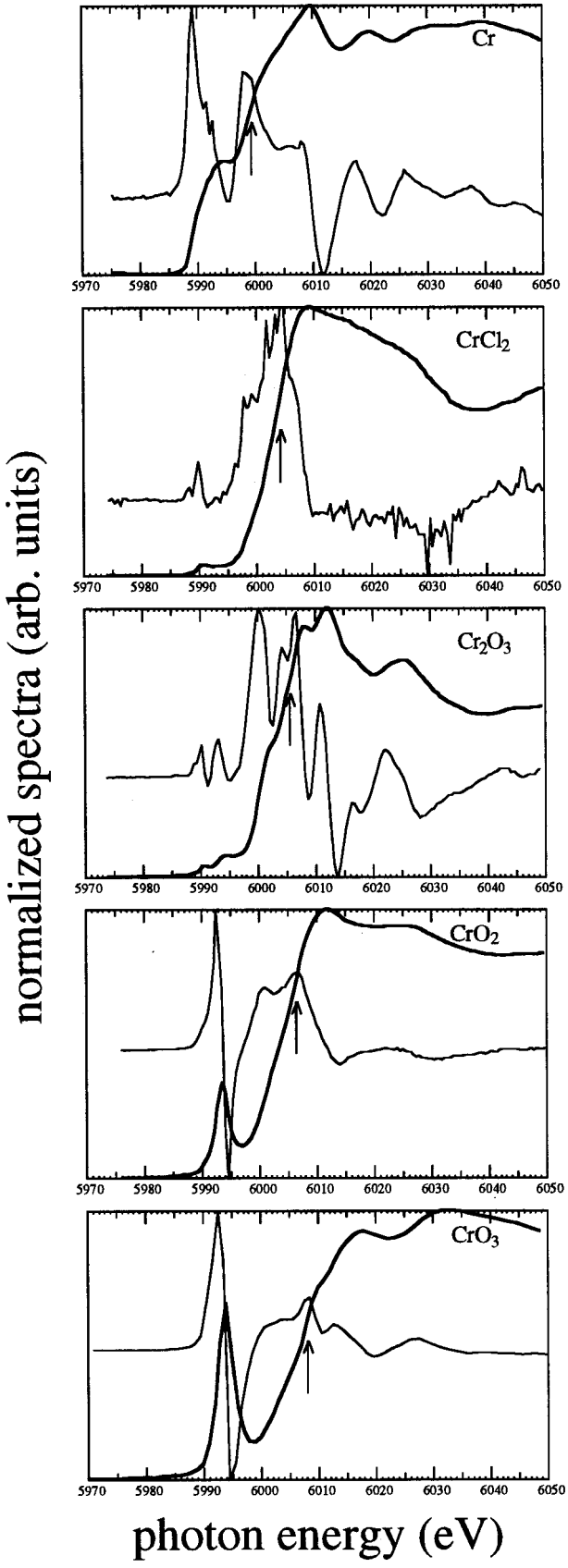

Figure 8. K-edge of Cr-doped standards and their derivative spectra.

(23) Durville, F.; Champagnon, B.; Duval, E.; Boulon, G. *J. Phys. Chem. Solids* **1985**, *46*, 701.
(24) Jia, W.; Liu, H.; Jaffe, S.; Yen, W. M.; Denker, B. *Phys. Rev. B* **1991**, *43*, 5234.

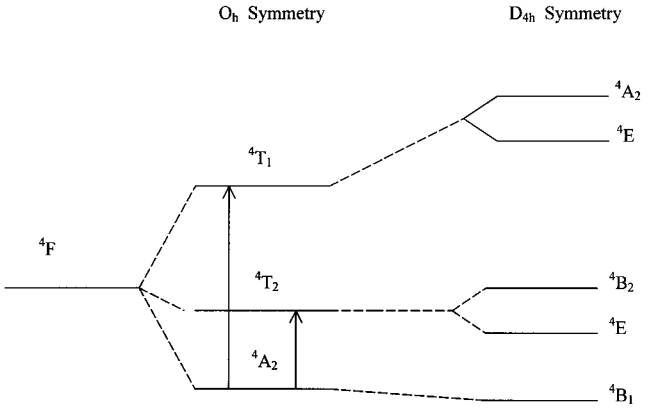

Figure 9. Energy level splitting of Cr^{3+} ($3d^3$ ion) in O_h and D_{4h} symmetries.

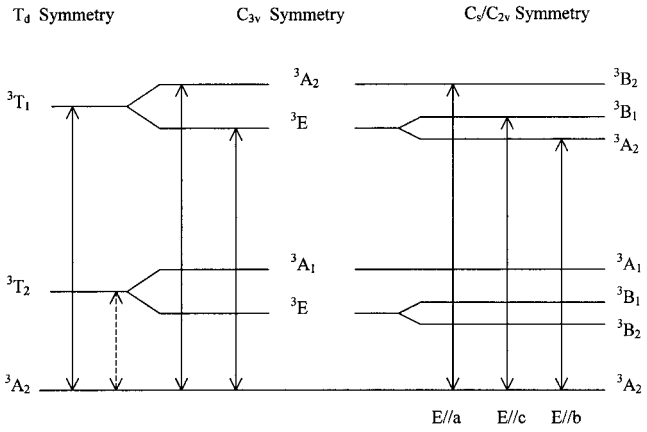

Figure 10. Energy level diagram of Cr^{4+} ($3d^2$ ion) in Td and lower symmetries.

values with those reported for Mg_2SiO_4, Ca_2SiO_4, and Ca_2GeO_4 indicates that all these materials crystallize in the orthorhombic form. It is known that γ-Ca_2SiO_4 and γ-Ca_2GeO_4 are structurally similar to forsterite, with the orthorhombic space group *Pbnm* with a tetrahedral site and two distinct octahedral sites.[25] Although Ca_2SiO_4 and Ca_2GeO_4 exhibit polymorphism crystallizing in the α and γ forms[25] in the high-temperature syntheses, these sol−gel syntheses yield only the γ-phases of Ca_2SiO_4 and Ca_2GeO_4, which is structurally equivalent to orthorhombic Mg_2SiO_4. Although structurally equivalent, a shift in the 2θ values to smaller angles indicates an expansion of the unit cell in the order $Mg_2SiO_4 < Ca_2SiO_4 < Ca_2GeO_4$.

Conversion to the crystalline orthorhombic phase changes the oxidation state and coordination of the chromium dopant. EPR spectra of Cr-doped Ca_2SiO_4 and Ca_2GeO_4 (Figure 5) show a single resonance with $g = 2.05 \pm 0.02$ and a half-width of 200 G. Although the half-width is significantly larger, the g value is within experimental error of that reported for aluminates,[14] alkyls,[26,27] and oxide glasses[28,29] containing tetrahedrally coordinated Cr^{4+} and is attributed to tetrahedrally coordinated Cr^{4+}. These resonances also resemble those observed in forsterite where Cr^{4+} formation has been attributed to a reaction between Cr^{3+} and excess oxygen defect centers.[28,29] In addition to the resonance attributed to tetrahederal Cr^{4+}, all Cr-doped forsterite samples prepared in these experiments exhibit an additional resonance with $g \approx 5$ and $g \approx 1.96$ that are (Figure 5) assigned to octahederally coordinated Cr^{3+}.[23,30]

XANES and EXAFS spectra yield similar results.[31] XANES spectra of different chromium standards show that the preedge feature for octahederally coordinated Cr^{3+} is weak or nonexistent (Cr_2O_3), whereas that for tetrahedrally coordinated Cr^{6+} (CrO_3) exhibits substantially higher intensity (Figure 8). This feature is normally present for Cr in an environment of lower symmetry like T_d. Here, Cr-MS and Cr-CG exhibit preedge peaks at 5994 eV (Figure 6) and 5993 eV (Figure 7) respectively, indicating the presence of tetrahedrally coordinated Cr^{4+} in both samples, but the substantially higher intensity of the Cr-CG preedge peak corresponds to a substantially larger amount of Cr^{4+} in this sample. The splitting of the preedge feature (Figures 6 and 7) arises from distortions in the symmetry of the crystal field surrounding the ion,[32] and the appearance of similar splitting suggests that similar distortions occur in both Cr-MS and Cr-CG. The energy onset of the main absorption, on the other hand, increases as the oxidation state of chromium increases as evident from Table 2. The near edge of the Cr-MS absorption is broad and can be fit with separate peaks at 6004.2 and 6006 eV, whereas the onset of the main absorption of Cr-CG lies at 6006.5 eV. Comparing these values with the onsets of the standards indicates the 6004.2 eV onset corresponds to octahederally coordinated Cr^{3+}, while that at 6006.5 eV corresponds to tetrahedrally coordinated Cr^{4+}. Consistent with the EPR, these results indicate the presence of both octahedrally coordinated Cr^{3+} and tetrahedrally coordinated Cr^{4+} in Cr-MS, while Cr-CG contains predominantly tetrahedrally coordinated Cr^{4+} with no detectable amount of octahedrally coordinated Cr^{3+}. These differences in composition are reflected in the electronic spectra.

In a tetrahedral field, the Cr^{4+} ground state, ^3F, splits into $^3A_2$, $^3T_2$, and $^3T_1$ levels with $^3A_2$ being the ground state (Figure 10).[11,24,33] One of the excited states of the free ions, ^3P transforms into $^3T_1$ (^3P). Previous studies of forsterite single crystals indicate that distortions reduce the symmetry of the Cr^{4+} coordination site, or the CrO_4^{4-} tetrahedron, from T_d to C_{3v} or C_s.[33] Under C_{2v} symmetry, the $^3T_1$ (^3F) level splits into $^3A_2$, $^3B_1$, and $^3B_2$, and the transitions to the individual levels, $^3A_2 \rightarrow {}^3A_2(^3T_1)$, $^3A_2 \rightarrow {}^3B_1(^3T_1)$, and $^3A_2 \rightarrow {}^3B_2(^3T_1)$, appear as polarized absorptions with polarizations along the *a*, *b*, and *c* crystal directions, respectively (Figure 10).[24,33] The

(25) Eysel, W.; Hahn, T. *Z. Kristallogr.* **1970**, *131*, S.322.
(26) Ward, G. A.; Krusi, W.; Bower, B. K.; Chien J. C. W. *J. Organomet. Chem.* **1972**, *42*, 143.
(27) Ward, G. A.; Bower, B. K.; Findlay, M.; Chien, J. C. W. *Inorg. Chem.* **1974**, *13*, 614.
(28) Murata, T.; Torisaka, M.; Takebe, H.; Morinaga, K. *J. Am. Ceram. Soc.* **1998**, *81*, 2135.
(29) Murata, T.; Torisaka, M.; Takebe, H.; Morinaga, K. *J. Non-Cryst. Solids* **1997**, *220*, 139.
(30) Ardelean, I.; Ilonca, Gh.; Peteanu, M.; Barbos, E.; Indrea, E. *J. Mater. Sci.* **1982**, *17*, 1988.
(31) Miyano, K. E.; Woick, J. C.; Sujatha Devi, P.; Gafney, H. D. *Appl. Phys. Lett.* **1997**, *71*, 1168.
(32) Wong, J.; Lytle, F. W.; Messmer, R. P.; Maylotte, D. H. *Phys. Rev. B* **1984**, *30*, 5596.
(33) Verdun, H. R.; Thomas, L. M.; Andrauskas, D. M.; Pinto, A. *OSA Proceeding on Tunable Solid State Lasers*;. Shand, M. L., Jenssen, H. P., Eds.; Optical Society of America: Woodbury, NY, 1989; Vol. 5, p 77.

bands appearing in the 380−430 nm region are assigned to the $^3A_2 \rightarrow {}^3T_1$ (^3P) transition of Cr^{4+}, while the bands appearing in the 600−700 nm region are assigned to the to spin-allowed $^3A_2 \rightarrow {}^3T_1(^3F)$ transition of Cr^{4+}. We will discuss the latter assignment later. Since Cr-MS contains a mixture of octahedrally coordinated Cr^{3+} and tetrahedrally coordinated Cr^{4+}, the higher intensity of the Cr^{4+} band around 400 nm in Cr-MS is attributed to an underlying $^4A_2 \rightarrow {}^4T_1$ transition of Cr^{3+}. The other ligand-field transition of Cr^{3+}, $^4A_2 \rightarrow {}^4T_2$, is assigned to the broad absorption centered at 660 nm in the spectrum of Cr-MS (Figure 4a) since Cr^{3+} exhibits a band in this energy range when incorporated into the sol or gel. In fact, a shoulder at ∼470 nm is evident on the long wavelength side of the Cr^{4+} transition that is assigned to $^4A_2 \rightarrow {}^4T_1$ transition of Cr^{3+}. This places the $^4A_2 \rightarrow {}^4T_1$ transition of octahedral Cr^{3+} in the region of the $^3A_2 \rightarrow {}^3T_1(^3P)$ transition of Cr^{4+} where it would contribute to the intensity of the $^3A_2 \rightarrow {}^3T_1$ transition of Cr^{4+}. Since the extinction coefficients of the $^4A_2 \rightarrow {}^4T_1$ and $^4A_2 \rightarrow {}^4T_2$ transitions of Cr^{3+} are similar, the underlying transition is expected to contribute an intensity similar to that of the $^4A_2 \rightarrow {}^4T_2$ occurring at 660 nm. Subtracting the latter yields a band intensity similar to that observed for the $^3A_2 \rightarrow {}^3T_1(^3P)$ transition of Cr^{4+} in Cr-CS and Cr-CG. Hence, the electronic spectrum of Cr-MS is a sum of the spectra of Cr(III) and Cr(IV), whereas those of Cr-CS and Cr-CG are dominated principally by Cr^{4+} transitions.

The bands appearing in the 600−700 nm region are attributed the spin-allowed $^3A_2 \rightarrow {}^3T_1$ transition of Cr^{4+}. The above transitions of Cr-CS and Cr-CG (Figure 3b and c) show a striking similarity, in both band energy and band shape with those of the polarized transitions of forsterite.[24] In fact, the immediate thought is to assign the transitions appearing at 604 nm in Cr-MS, 677 nm in Cr-CS and 718 nm in Cr-CG to the $^3A_2 \rightarrow {}^3B_2(^3T_1)$, $^3A_2 \rightarrow {}^3B_1(^3T_1)$ and $^3A_2 \rightarrow {}^3A_2(^3T_1)$ transitions, respectively. However, the spectra recorded on our experiments are of randomly arrayed microcrystalline powders, where there is no preferred orientation that could give rise to polarization of the electronic transitions. Instead, the bands appearing at 604 nm in Cr-MS, 677 nm in Cr-CS and 718 nm in Cr-CG and the shoulders that appear on the long wavelength sides of these bands must be composites of all polarizations. The lower energy transitions occurring at 667 and 714 nm in the Cr-MS spectrum, exhibit an energy spacing similar to that observed in the polarized single-crystal spectrum of Cr-MS and are tentatively assigned to the $^3A_2 \rightarrow {}^3B_1(^3T_1)$ and $^3A_2 \rightarrow {}^3A_2(^3T_1)$ components. As noted above, however, the band at 660 nm in the Cr-MS spectrum is also thought to possess some intensity from the $^4A_2 \rightarrow {}^4T_2(^3T_1)$ transition of octahedral Cr^{3+}. This band appears in this energy region in spectra of the Cr^{3+}-doped MS sols and gels, and EPR and XANES confirm the presence of both octahedrally coordinated Cr^{3+} and tetrahederally coordinated Cr^{4+} in the Cr-MS ceramics. Although the longer wavelength bands are not as well resolved in the Cr-CS and Cr-CG spectra, the 677 and 724 nm bands in the Cr-CS spectrum (Figure 3b) exhibit an energy spacing similar to that in Cr-MS and are likewise assigned to the $^3A_2 \rightarrow {}^3B_1(^3T_1)$ and $^3A_2 \rightarrow {}^3A_2(^3T_1)$ transitions. Similarly, the bands at 718 and 825 nm in the Cr-CG spectrum are also tentatively assigned to these transitions since the shift to longer wavelengths of each series of bands parallels the average field strength in the respective olivines. These transitions are followed by low intensity transitions at 1092 nm in Cr-MS and 1207 nm in Cr-CS and Cr-CG that are assigned to the electric-dipole forbidden transition $^3A_2 \rightarrow {}^3T_2$.

The assignment of the well-defined shoulders present on the high energy sides of the 604 nm band of Cr-MS, the 677 nm band of Cr-CS, and the 718 nm band of Cr-CG is not clear. In appearance and energy, the progression is analogous to that reported for the splitting of the $^3T_1$ level of Cr^{4+} in forsterite due to the reduction in symmetry to C_s. Hence these transitions may correspond to the transition from the triplet to the corresponding singlets.[24]

Room-temperature emission spectra of Cr-MS reflect the presence of both octahederal Cr^{3+} and tetrahedral Cr^{4+}. Excitation of Cr-MS with either 670 or 800 nm light leads to weak emission with a maximum at 950 nm, and much higher intensity emission centered at 1158 nm (Figure 4). Excitation with 1064 nm light, however, leads to only the 1158 nm emission. The 950 nm emission is assigned to either the $^2E \rightarrow {}^4A_2$ phosphorescence, or $^4T_2 \rightarrow {}^4A_2$ fluorescence from octahedrally coordinated Cr^{3+} since the emission occurs only with higher energy excitation. Since the 1158 nm emission occurs with 1064 nm excitation, which corresponds to the $^3A_2 \rightarrow {}^3T_2$ transition of tetrahedral Cr^{4+}, this emission is assigned to the corresponding $^3T_2 \rightarrow {}^3A_2$ fluorescence. Regardless of the excitation wavelength, excitation of Cr-CS and Cr-CG leads to single emissions with maxima at 1275 and 1285 nm, respectively. The emissions show a red shift of 792 cm^{-1} on going from Mg_2SiO_4 to Ca_2SiO_4 and a further 853 cm^{-1} shift on going from Mg_2SiO_4 to Ca_2GeO_4. Since the shift to longer wavelength of the emission parallels the shift to longer wavelength of the $^3A_2 \rightarrow {}^3T_2$ absorptions, the 1275- and 1285- nm emissions are assigned to the corresponding $^3T_2 \rightarrow {}^3A_2$ fluorescence. The shift to longer wavelengths further suggests that the tetrahedrally coordinated Cr^{4+} experiences a weaker field in Ca_2GeO_4 and increasingly stronger fields in Ca_2SiO_4 and Mg_2SiO_4. This is further supported by the X-ray data where the 2θ values shift toward the low angle side as one moves from Mg_2SiO_4 to Ca_2SiO_4 to Ca_2GeO_4 indicating a unit cell expansion. Consistent with the larger amount of tetrahedral Cr^{4+} present in Cr-CS and Cr-CG, at the same loading, i.e., Cr/Si or Cr/Ge equal to 0.01%, and same excitation wavelength, 670 nm, the emission intensity from Cr-CS and Cr-CG is significantly higher than the long wavelength emission from Cr-MS. Further experiments, particularly polarized absorption spectroscopy, of these different olivines are needed to confirm the above assignments and clarify the origins of some of the absorption and emission features of the systems.

5. Conclusions

The absorption and emission properties of these olivine-structured materials reflect different oxidation states and coordination of the Cr-dopant. EPR and electronic spectroscopy show that octahederally coordinated Cr^{3+} ion is present in each gel, but calcination at 850 °C converts the gel to microcrystalline materials

with corresponding changes in chromium oxidation state and coordination. X-ray analysis confirms each gel converts to the analogously structured orthorhombic crystalline form. However, converting Ca_2GeO_4 and Ca_2SiO_4 gels containing octahederally coordinated Cr^{3+} to orthorhombic ceramics yield predominantly tetrahederally coordinated Cr^{4+}, whereas converting the doped Mg_2SiO_4 to a ceramic yields a mixture of octahedrally Cr^{3+} and tetrahedrally coordinated Cr^{4+}. Consistent with expectations based on the sizes of the relevant ions, Ca_2GeO_4 and Ca_2SiO_4 favor formation of tetrahederally coordinated Cr^{4+}. However, electronic absorption and emission spectra of the different olivines, which reflect these differences in composition, show that the Cr^{4+} tetrahedral coordination sites are distorted with the average field strength declining with increasing size of the unit cell.

Acknowledgment. Support of this research by DOD/AFSOR (F49620-94-1-0209), the National Science Foundation (DMR-9314033), the CUNY Collaborative Research Incentive Grant Program and the New York state Center of Advanced Technology is gratefully acknowledged. P.S.D. thanks the Director, CG&CRI, Calcutta, for providing the opportunity to work on this collaborative project.

CM990730+